

Bidirectional Self-Folding with Atomic Layer Deposition Nanofilms for Microscale Origami

Baris Bircan, Marc Z. Miskin, Robert J. Lang, Michael C. Cao, Kyle J. Dorsey, Muhammad G. Salim, Wei Wang, David A. Muller, Paul L. McEuen, and Itai Cohen*

Cite This: *Nano Lett.* 2020, 20, 4850–4856

Read Online

ACCESS |

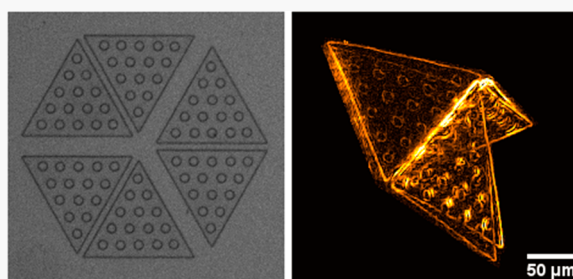
Metrics & More

Article Recommendations

Supporting Information

ABSTRACT: Origami design principles are scale invariant and enable direct miniaturization of origami structures provided the sheets used for folding have equal thickness to length ratios. Recently, seminal steps have been taken to fabricate microscale origami using unidirectionally actuated sheets with nanoscale thickness. Here, we extend the full power of origami-inspired fabrication to nanoscale sheets by engineering bidirectional folding with 4 nm thick atomic layer deposition (ALD) $\text{SiN}_x\text{-SiO}_2$ bilayer films. Strain differentials within these bilayers result in bending, producing microscopic radii of curvature. We lithographically pattern these bilayers and localize the bending using rigid panels to fabricate a variety of complex micro-origami devices. Upon release, these devices self-fold according to prescribed patterns. Our approach combines planar semiconductor microfabrication methods with computerized origami design, making it easy to fabricate and deploy such microstructures en masse. These devices represent an important step forward in the fabrication and assembly of deployable micromechanical systems that can interact with and manipulate micro- and nanoscale environments.

KEYWORDS: Atomic layer deposition, origami, self-assembly, microstructures, nanofabrication



Because of their scale invariance, origami design principles have been used to create complex systems across various sizes such as deployable solar panels on spacecraft,^{1,2} centimeter scale programmable materials^{3,4} and robots,^{5,6} and micro-electromechanical systems (MEMS).⁷ At the microscale, origami has proven to be especially advantageous, as it has allowed the use of planar lithographic fabrication methods to build 3D structures that remain inaccessible to other manufacturing processes. Within the past decade, folding at the microscale has been demonstrated using metallic thin films,^{8,9} polymers,^{10,11} and atomically thin films of hard materials.^{12–15}

As a result of their high Young's modulus and low bending stiffness, ultrathin films of hard materials are an excellent material choice for self-folding micro-origami. When fabricated at nanoscale thicknesses, these films can repeatedly and elastically deform to micron scale radii of curvature¹⁶ while producing sufficient force output to lift rigid panels 1000-times their thickness.¹⁷ Atomic layer deposition (ALD) enables the fabrication of oxide and nitride films with nanometer thickness, high mechanical integrity, high uniformity, and low pinhole defect density.^{18–21} Thus, this technology opens the door to a new generation of atomically thin sheets that define the smallest possible size scale for self-folding. Recent work has demonstrated ALD-based, 2 nm thick unidirectional bending actuators

to build elementary self-folding microstructures like tetrahedra and cubes.¹⁴

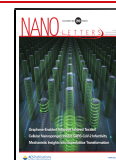
In general, the algorithmic mapping of a 3D shape to a fold pattern requires the assignment of fold angles ranging from -180° to $+180^\circ$.^{22,23} Therefore, unidirectional fold actuation limits the space of shapes that can be fabricated to relatively simple ones. Bidirectional folding is required to create combinations of mountain (downward) and valley (upward) folds found in complex origami designs (Figure 1A).²⁴ While inorganic ALD films have emerged as a promising class of materials for creating microscale folds, systems based on these materials have not yet demonstrated bidirectional folding for origami-based 3D self-assembly.²⁵

Here, we present 4 nm thick, ALD oxide-nitride bilayer films that achieve bidirectional bending, and we use these films to develop a scalable microfabrication process that can be generalized to create rigidly foldable²⁶ origami. The ultrathin ALD bilayers at the center of our approach convert an internal strain mismatch into a bending response. Provided that a certain

Received: February 24, 2020

Revised: June 8, 2020

Published: June 11, 2020



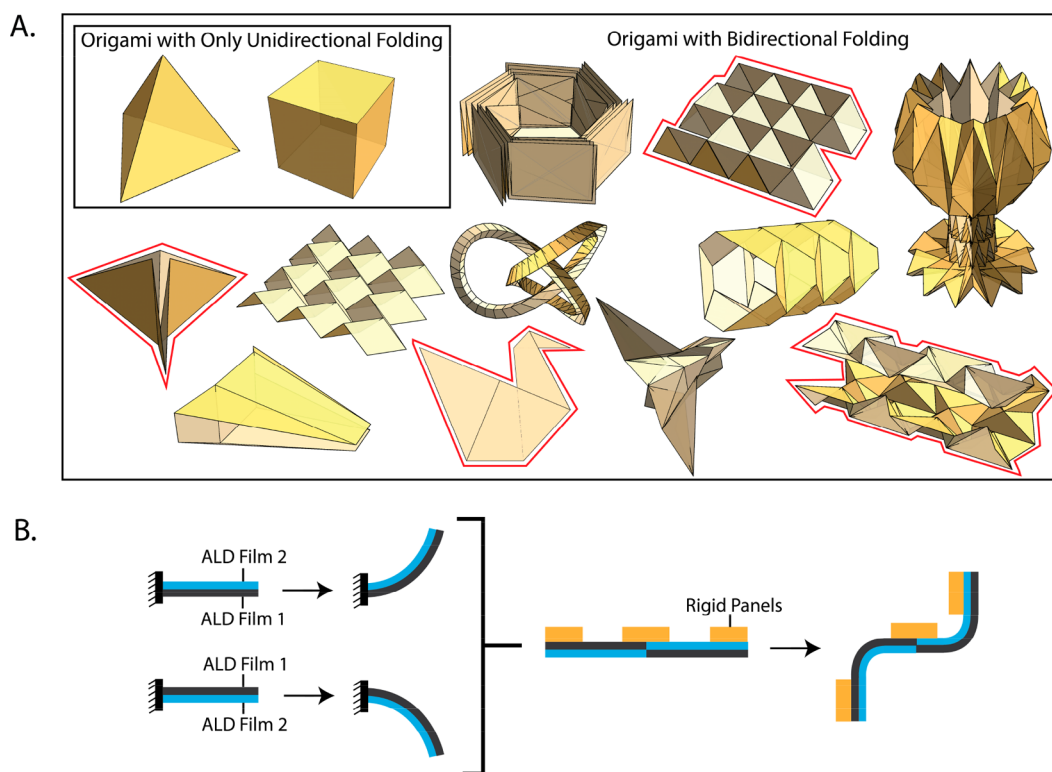


Figure 1. Bidirectional folding with atomic layer deposition (ALD) bilayer films. Mapping of an arbitrary 3D shape to an origami fold pattern requires the assignment of fold angles ranging from -180° to $+180^\circ$. As a result, unidirectional fold actuation limits the space of shapes that can be fabricated to relatively simple ones (A). Bidirectional folding is required to create combinations of mountain (downward) and valley (upward) folds found in complex origami designs. We choose to experiment with the four designs highlighted in red to demonstrate our approach can create microscale origami of variable complexity. To engineer self-folding at the microscale, we use ALD bilayer films, which convert an internal strain mismatch into a bending response (B). If a certain bilayer stack of ALD films produces bending in one direction, the stacking order can be inverted to create bending in the opposite direction. We create bidirectional folding by combining sheets that bend in different directions and adding rigid panels to localize bending.

bilayer stack of ALD films bends in one direction, the stacking order can be inverted to produce bending in the opposite direction. To create bidirectional folding, we combine ALD bilayers that bend in opposite directions and add rigid panels to localize bending (Figure 1B). Our fabrication process is based entirely on conventional semiconductor manufacturing techniques and lets us take advantage of lithographic methods to pattern and release our microscale origami devices in parallel. When released into solution, these devices self-fold into configurations defined by prescribed fold patterns. Using this approach, we fabricate a variety of complex micro-origami devices, which can withstand highly corrosive acidic environments and processing temperatures up to 150°C . The development of these self-folding nanofilms, together with a process that can be generalized to create arbitrarily complex origami, extends the full power of origami-inspired fabrication to nanoscale sheets.

We identify ALD SiN_x and SiO_2 as suitable materials for use in our micro-origami devices due to their low growth stresses and similar Young's moduli.²⁷ To obtain the smallest possible sheet thickness and maximum bending deformation, while ensuring that fully nucleated ALD films can be reproducibly deposited, we fabricate bilayers consisting of 2 nm of SiO_2 and 2 nm of SiN_x . Figure 2A (and Supporting Video 1) shows a hinge made with a SiN_x (bottom)- SiO_2 (top) bilayer and a flat panel made of SU-8 polymer. When released in solution, this hinge folds upward, thus identifying the film stacking order that will be used for valley (upward) folding.

Residual stresses form within the SiN_x and SiO_2 films due to the nucleation and growth processes that occur during atomic layer deposition, and thermal stresses form due to the elevated growth temperatures and the mismatch between the thermal expansion coefficients of the films. A combination of these stress components gives rise to the intrinsic curvature of the bilayer, which we localize to create folds. We measure this curvature to be $0.1\ \mu\text{m}^{-1}$ for folding in both directions, which is consistent with a strain on the order of 0.01% given the thickness of the bilayer (details on bilayer curvature characterization can be found in the SI). Since the strains present are two orders of magnitude below the fracture strains for silicon nitride and silicon dioxide,^{28,29} the hinge operates elastically, demonstrating full recovery after being deformed by an applied force. Electron energy loss spectroscopy (EELS) (Figure 2B) and X-ray photoelectron spectroscopy (XPS) (Figure 2C) on the ALD film stack used in this hinge confirm that the bilayer consists of approximately 2 nm thick layers of SiN_x and SiO_2 (details on ALD film stack characterization can be found in the SI).

Combined with knowledge of the ALD bilayer's intrinsic curvature, the ability to invert the bending direction by changing the process order makes the fabrication of mountain (downward) and valley (upward) folds on separate substrates relatively straightforward. However, the similar etch behavior of the two ultrathin ALD films presents a challenge for fabricating complex patterns of alternating fold direction on a microscopic device. During fabrication, sequential photolithography and etching steps risk damaging or completely removing previously patterned parts of each device. Here, we develop a fabrication

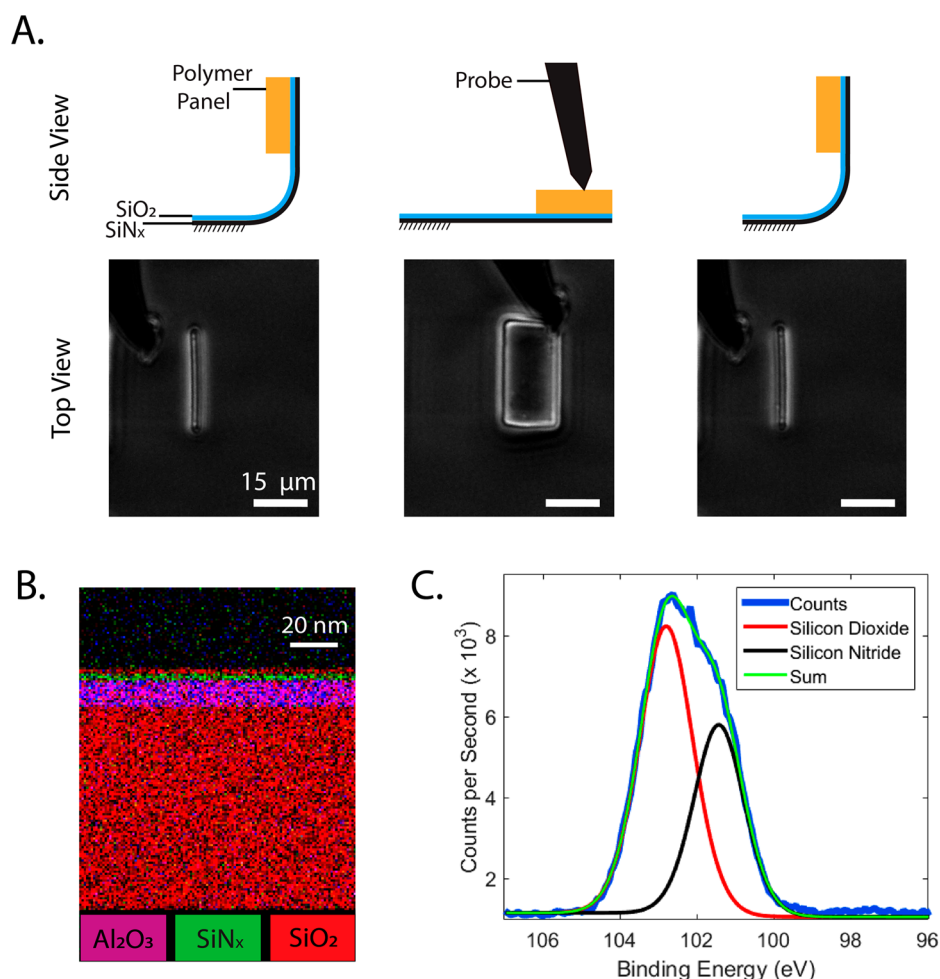


Figure 2. Operation and structure of an ALD SiN_x-SiO₂ hinge. A hinge made with an ALD SiN_x (bottom)-SiO₂ (top) bilayer and a flat SU-8 panel folds upward when released (A), identifying the device structure needed for valley folding. The bilayer hinge operates elastically, demonstrating full recovery after being deformed by a micromanipulator probe. EELS analysis (B) of the ALD bilayer confirms that the ALD nitride and oxide films making up the bilayer meet their target thickness of 2 nm. Elemental signals for oxygen (red), aluminum (blue), and nitrogen (green) have been isolated to create the color-coded EELS map. The bilayer is seen on top of a 10 nm thick layer of Al₂O₃, which is colored pink due to a combination of blue (aluminum) and red (oxygen). High resolution XPS scans of the ALD film stack further confirm the internal structure of the bilayer (C). Photoelectron counts from the film stack (blue) are fit well by the sum (green) of two Voigt profiles centered at Si 2p binding energy values corresponding to SiO₂ (red) and SiN_x (black) (details on ALD film stack characterization can be found in the SI).

process that incorporates an aluminum etch mask to protect device layers during processing without sacrificing geometrical complexity. This approach allows us to reliably create combined bidirectional folds, where fold angles can range from -180° to $+180^\circ$.

The process flow needed to fabricate a general microscopic origami shape is outlined in Figure 3. We start by thermally evaporating an aluminum release layer onto a substrate. Then we grow an ALD SiO₂-SiN_x film stack. Next, we thermally evaporate another layer of aluminum to be used as an etch mask in subsequent steps (Figure 3A). We spin coat the substrate with a standard positive tone photoresist and use contact photolithography to define the mountain (downward) fold regions of the origami shape. We then perform plasma etching to transfer the photoresist pattern into the aluminum etch mask and the ALD stack underneath it (Figure 3B,C). We remove the photoresist by soaking the substrate in solvent overnight.

Next, we deposit an inverted SiN_x-SiO₂ ALD film stack (Figure 3D). The conformal nature of the ALD process results in a fully coated substrate, which ensures the ALD films making up each device are continuous. We spin coat the substrate with

positive photoresist and use contact photolithography followed by plasma etching to pattern the inverted bilayer film (Figure 3E,F). This step defines the ALD hinges that make up the valley (upward) folds as well as the regions where the flat panels will be placed. During this patterning step, the mountain (downward) fold regions are protected from the plasma by the aluminum mask. We leave a 3–5 μm overlap between the mountain and valley photoresist patterns to ensure the ALD sheets making up each device are continuous. After pattern transfer, we remove the photoresist by soaking the substrate in solvent overnight.

Next, we spin coat the wafer with SU-8 photoresist and use contact photolithography to pattern 1 μm thick flat panels (Figure 3G). Using the measured thicknesses and known elastic constants of our materials,^{17,27,30} we estimate that the bending stiffness $Yt^3/[12(1-\nu^2)]$ (Y , Young's modulus; t , thickness; ν , Poisson's ratio) of the SU-8 panels is five orders of magnitude larger than that of the self-folding ALD sheets. Therefore, the SU-8 panels are effectively rigid compared to the ALD hinges and can be used to define flat facets for each origami shape.

Lastly, we use an HCl wet etch to dissolve the aluminum release layer and etch mask to release the origami devices into

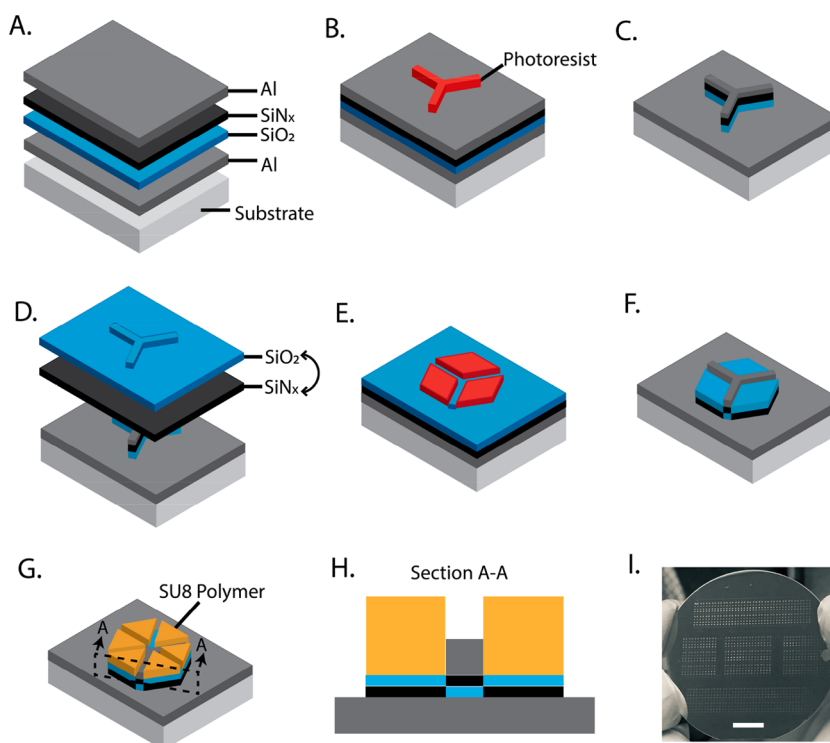


Figure 3. Process flow to fabricate self-folding micro-origami with ALD nanofilms. Our process can be used to microfabricate any rigidly foldable origami pattern that folds simultaneously. The steps required to fabricate a micro-origami device are described using the origami hexagon as an example: Deposit an aluminum release layer on a transparent substrate, followed by an ALD SiO_2 - SiN_x film stack and another layer of aluminum for etch masking (A). Use photolithography to define the mountain (downward) fold regions of the origami shape (B). Perform plasma etching and transfer the photoresist pattern into the aluminum etch mask and the ALD stack underneath it (C). Deposit an inverted SiN_x - SiO_2 ALD film stack and coat the entire substrate (D). Use photolithography to define the ALD hinges that make up the valley (upward) folds as well as the regions where the flat panels will be placed (E). Use plasma etching to pattern the inverted ALD bilayer, while the aluminum mask protects the previously patterned mountain fold regions (F). Use photolithography to pattern $1\ \mu\text{m}$ thick flat SU-8 panels (G). Device cross section after processing is completed (H). Unreleased origami devices on a processed two-inch wafer are seen as an array of points to the naked eye (I). Scale bar is 1 cm. Immersing the wafer in an HCl solution removes the aluminum release layer and etch mask, allowing the devices to deploy and self-fold.

solution, where they freely fold. All device layers are designed to have aligned holes exposing the release layer to the etch solution, so that undercut time during the release process is reduced.

Our fabrication approach is applicable to any rigidly foldable origami pattern that folds simultaneously, and allows us to design and construct a large variety of structures. We use an extended version of the Tessellatica³¹ package to automate the lithography mask design process. Through this software package, fold patterns modeled in Tessellatica are converted into design files for a set of three lithography masks. We then directly incorporate each mask into the corresponding lithography step in our process to microfabricate the fold patterns. The Tessellatica package used in generating our lithography masks can be found under ref 32.

The software we use to create our lithography masks converts fold lines of infinitesimal width into hinges with finite width. The direction for each fold is determined by the ALD bilayer stack order at the fold location, and the magnitude of the fold angle is given by the ratio of the exposed length between rigid panels to the intrinsic radius of curvature produced by the bilayer.

Microscopic origami devices of variable complexity made using this approach are shown in Figure 4. In each row, from left to right, we show the fold pattern for an origami shape, a render of the target 3D shape, a finite element model of the self-folding device, the micro-origami device attached to the substrate in its flat state, and the micro-origami device in its folded state. We image our devices with an optical microscope and create the

images of the folded devices by taking a 2D projection of images collected from different focal planes. For devices with larger panels, such as the ones in Figure 4A and B, we use image slices obtained with a confocal microscope to create the projections to better capture the 3D geometries. Since the self-folding ALD sheets we develop here are transparent, only the flat SU-8 panels on each device are visible in the micrographs. Knowing that the SU-8 panels are connected by transparent ALD hinges of finite length in our finished devices, we infer the overall 3D shapes from the relative positions of the panels. We include finite element models of the devices together with their micrographs to visualize the overall 3D shapes by highlighting the ALD sheets, which are otherwise not visible.

The simplest structure we demonstrate is the origami hexagon (Figure 4A), which has six folds. The apparent discontinuity of the bottom pair of edges in the folded device is an artifact of the transparency of the ALD sheets since the two adjacent SU-8 panels are visible, but the transparent curved hinge connecting them is not.

As a more complex example, we show the rigidly foldable duck (Figure 4B, 17 folds), which is less than half the size of the current state-of-the-art micro-origami bird.¹¹ Because of the increased density of folds near the head of the duck, the microscopic device design we obtain from our software consists only of ALD bilayers near the head of the duck, which makes this region transparent. Since we can verify correct kinematic

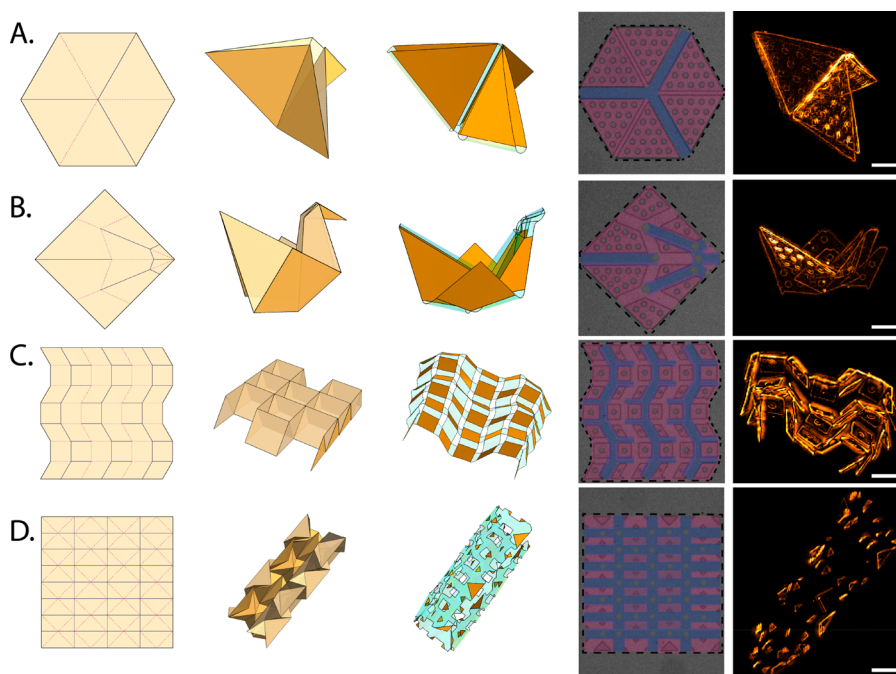


Figure 4. Self-folding micro-origami made with ALD nanofilms. ALD $\text{SiN}_x\text{-SiO}_2$ bilayer films can be used to fabricate microscale origami of variable complexity. From top to bottom, the examples we show here are the origami hexagon (A) with 6 folds, the rigidly foldable duck (B) with 17 folds, the spacer Miura-ori (C) with 71 folds, and the waterbomb tessellation (D) with 120 folds. The leftmost column of the figure shows fold patterns corresponding to each origami shape, with mountain (downward) fold lines drawn in blue and valley (upward) fold lines drawn in pink. The second to left column shows renders of each folded origami shape. The middle column shows finite element models of the expected folded device configurations, with rigid panels represented in orange and the transparent self-folding sheets represented in light blue. We note that the finite element models include holes in their vertices to avoid singularities in computation (model details can be found in the SI). The second to the right column shows microscale origami devices attached to the substrate in their flat state, with dashed lines outlining each device. The transparent ALD sheets making up the devices are visualized using false color. Regions with SiO_2 (bottom)- SiN_x (top) bilayers are shaded blue, and regions with SiN_x (bottom)- SiO_2 (top) bilayers are shaded pink. Vertices that have had material removed from them are left uncolored. The grid of holes evident in the SU-8 panels is introduced into all the device layers to expose the release layer to the etch solution and reduce the time needed to undercut the devices during the wet release process. The rightmost column shows microscale origami devices after they have been released and allowed to self-assemble into their folded configurations, with the SU-8 panels colored orange. Scale bars are $50 \mu\text{m}$.

positioning of all the SU-8 panels, we conclude that the device has self-assembled as designed.

Lastly, we demonstrate that our fabrication process can also be used to build structures that are an order of magnitude more complex, such as the spacer Miura-ori (Figure 4C, 71 folds), and the waterbomb (Figure 4D, 120 folds) tessellation, which has the same diameter as a human hair. The folded form of the spacer Miura-ori device has SU-8 panels tilting alternately upward and downward, separated by fully flat-folded regions, as designed. Because of the high density of folds in the waterbomb tessellation, the conversion of this origami design into a microscopic device requires that most of the structure consists of only ALD bilayers. Even though the visible SU-8 panels constitute only a small fraction of the overall area, we can verify that the distribution of folded regions gives rise to a cylindrical folded form with the correct aspect ratio and conclude that the device has self-assembled as designed. Our technique thus demonstrates the ability to design and fabricate microscale origami ranging from relatively simple shapes with less than 10 folds to complicated tessellations with more than 100 folds.

When process limitations are considered, stiction is the most important factor affecting our device yield. During the wet release process, adhesion between the substrate and the origami devices can lead to partial release of devices, which prevents full deployment and assembly into the correct target geometries. Similarly, the self-folding ALD sheets can stick to themselves

upon contact, resulting in devices that get stuck in a misfolded position, preventing assembly into the correct target geometries. We introduce surfactant into the solution environment to reduce these impacts of stiction. The resulting device yield varies from about 50% for simple geometries like the hexagon to less than 10% for complex geometries like the spacer Miura-ori. To minimize fabrication costs, we dice our substrates into $2 \text{ cm} \times 2 \text{ cm}$ pieces containing about a thousand devices each, and we experiment on one piece at a time. The substrate and die sizes are not limited by any of our fabrication steps, and the process can easily be scaled up by using larger substrates.

Overall, our approach establishes a complete toolkit for origami-inspired microfabrication with hard materials: using software tailored for our ALD sheets, any fold pattern can be converted into a set of lithography masks, which can be directly included into our process to mass fabricate the designs at the microscale. This process opens the door to a whole class of deployable origami-inspired microscale mechanisms and machines that can explore and interact with their environment.

The use of ultrathin ALD bilayers for origami-inspired microfabrication establishes a strong foundation for future work. The process we have developed in this work can easily be generalized to include bilayers and trilayers made up of any ALD material as long as the individual ALD films have sufficiently small internal stress gradients so that the only significant curvature formed is due to the strain mismatch between the two

layers. The wide material palette offered by ALD,³³ combined with surface functionalization methods, provides a way to incorporate various capabilities into our devices such as voltage, chemistry, temperature, and biomolecule-based sensing and actuation. Stepwise fold actuation mechanisms can be introduced to enable sequential folding, allowing more reliable folding pathways^{34,35} and even more complicated origami structures. Since our fabrication process is entirely carried out in a cleanroom using semiconductor processing tools, it can also be extended to include on-board microelectronics or magnets^{17,36} to control and actuate our self-assembled structures. If there is need to remove the devices from liquid and into atmosphere, critical point drying can be employed to avoid damage due to surface tension forces. The integration of these capabilities will make our micro-origami devices a powerful tool for interacting with and manipulating environments at the micrometer and nanometer scales.

■ ASSOCIATED CONTENT

SI Supporting Information

The Supporting Information is available free of charge at <https://pubs.acs.org/doi/10.1021/acs.nanolett.0c00824>.

Sample fabrication details, ALD bilayer characterization, finite element modeling, supporting video description (PDF)

Video of pushing on ALD hinge with micromanipulator probe (AVI)

■ AUTHOR INFORMATION

Corresponding Author

Itai Cohen – *Laboratory of Atomic and Solid State Physics and Kavli Institute at Cornell for Nanoscale Science, Cornell University, Ithaca, New York 14853, United States;*
orcid.org/0000-0001-9218-043X; Email: ic64@cornell.edu

Authors

Baris Bircan – *School of Applied and Engineering Physics, Cornell University, Ithaca, New York 14853, United States;*

orcid.org/0000-0002-3398-2480

Marc Z. Miskin – *Laboratory of Atomic and Solid State Physics and Kavli Institute at Cornell for Nanoscale Science, Cornell University, Ithaca, New York 14853, United States*

Robert J. Lang – *Robert J. Lang Origami, Alamo, California 94507, United States*

Michael C. Cao – *School of Applied and Engineering Physics, Cornell University, Ithaca, New York 14853, United States*

Kyle J. Dorsey – *School of Applied and Engineering Physics, Cornell University, Ithaca, New York 14853, United States*

Muhammad G. Salim – *Cornell Center for Materials Research, Cornell University, Ithaca, New York 14853, United States*

Wei Wang – *Laboratory of Atomic and Solid State Physics, Cornell University, Ithaca, New York 14853, United States*

David A. Muller – *School of Applied and Engineering Physics and Kavli Institute at Cornell for Nanoscale Science, Cornell University, Ithaca, New York 14853, United States*

Paul L. McEuen – *Laboratory of Atomic and Solid State Physics and Kavli Institute at Cornell for Nanoscale Science, Cornell University, Ithaca, New York 14853, United States*

Complete contact information is available at:

<https://pubs.acs.org/doi/10.1021/acs.nanolett.0c00824>

Author Contributions

B.B., M.Z.M., P.L.M., and I.C. conceived the experiments. B.B. fabricated the samples and performed the experiments with assistance from M.Z.M. and under P.L.M.'s and I.C.'s supervision. R.J.L. contributed origami fold patterns and developed software for automated lithography mask design. M.C.C. and K.J.D. performed cross-sectional imaging and thickness characterization of ALD bilayers under D.A.M.'s supervision. M.G.S. performed XPS analysis of ALD bilayers. W.W. created finite element models of origami shapes. B.B. and I.C. wrote the manuscript with consultation from all authors.

Funding

This work made use of the Cornell Center for Materials Research Shared Facilities, which are supported through the NSF MRSEC program (DMR-1719875). This work was supported by the U.S. Army Research Office (ARO W911NF-18-1-0032), the Cornell Center for Materials Research with funding from the NSF MRSEC program (DMR-1719875), the Watt W. Webb Fellowship at Kavli Institute at Cornell for Nanoscale Science, and performed in part at the Cornell NanoScale Science and Technology Facility (CNF), a member of the National Nanotechnology Coordinated Infrastructure (NNCI), which is supported by the National Science Foundation (Grant NNCI-1542081).

Notes

The authors declare no competing financial interest.

■ ACKNOWLEDGMENTS

We thank Michael Reynolds, Tanner Pearson, Alejandro Cortese, Samantha Norris, Qingkun Liu, Meera Ramaswamy, and Samuel Whitehead for insightful discussions.

■ ABBREVIATIONS

ALD, atomic layer deposition; EELS, electron energy loss spectroscopy; XPS, X-ray photoelectron spectroscopy

■ REFERENCES

- (1) Zirbel, S. A.; Lang, R. J.; Thomson, M. W.; Sigel, D. A.; Walkemeyer, P. E.; Trease, B. P.; Magleby, S. P.; Howell, L. L. Accommodating Thickness in Origami-Based Deployable Arrays. *J. Mech. Des.* **2013**, *135* (11), 111005.
- (2) Zirbel, S. A.; Wilson, M. E.; Magleby, S. P.; Howell, L. L. An Origami-Inspired Self-Deployable Array. *American Society of Mechanical Engineers Digital Collection*, 2014. DOI: 10.1115/SMASIS2013-3296.
- (3) Silverberg, J. L.; Evans, A. A.; McLeod, L.; Hayward, R. C.; Hull, T.; Santangelo, C. D.; Cohen, I. Using Origami Design Principles to Fold Reprogrammable Mechanical Metamaterials. *Science* **2014**, *345* (6197), 647–650.
- (4) Hawkes, E.; An, B.; Benbernou, N. M.; Tanaka, H.; Kim, S.; Demaine, E. D.; Rus, D.; Wood, R. J. Programmable Matter by Folding. *Proc. Natl. Acad. Sci. U. S. A.* **2010**, *107* (28), 12441–12445.
- (5) Felton, S.; Tolley, M.; Demaine, E.; Rus, D.; Wood, R. A Method for Building Self-Folding Machines. *Science* **2014**, *345* (6197), 644–646.
- (6) Miyashita, S.; Guitron, S.; Ludersdorfer, M.; Sung, C. R.; Rus, D. An Untethered Miniature Origami Robot That Self-Folds, Walks, Swims, and Degrades. In *2015 IEEE International Conference on Robotics and Automation (ICRA)*, 2015; pp 1490–1496. DOI: 10.1109/ICRA.2015.7139386.
- (7) Rogers, J.; Huang, Y.; Schmidt, O. G.; Gracias, D. H. Origami MEMS and NEMS. *MRS Bull.* **2016**, *41* (2), 123–129.
- (8) Cho, J.-H.; Gracias, D. H. Self-Assembly of Lithographically Patterned Nanoparticles. *Nano Lett.* **2009**, *9* (12), 4049–4052.

- (9) Bassik, N.; Stern, G. M.; Gracias, D. H. Microassembly Based on Hands Free Origami with Bidirectional Curvature. *Appl. Phys. Lett.* **2009**, *95* (9), No. 091901.
- (10) Jamal, M.; Zarafshar, A. M.; Gracias, D. H. Differentially Photo-Crosslinked Polymers Enable Self-Assembling Microfluidics. *Nat. Commun.* **2011**, *2* (1), 1–6.
- (11) Na, J.-H.; Evans, A. A.; Bae, J.; Chiappelli, M. C.; Santangelo, C. D.; Lang, R. J.; Hull, T. C.; Hayward, R. C. Programming Reversibly Self-Folding Origami with Micropatterned Photo-Crosslinkable Polymer Trilayers. *Adv. Mater.* **2015**, *27* (1), 79–85.
- (12) Bles, M. K.; Barnard, A. W.; Rose, P. A.; Roberts, S. P.; McGill, K. L.; Huang, P. Y.; Ruyack, A. R.; Kevek, J. W.; Kobrin, B.; Muller, D. A.; McEuen, P. L. Graphene Kirigami. *Nature* **2015**, *524* (7564), 204–207.
- (13) Xu, W.; Qin, Z.; Chen, C.-T.; Kwag, H. R.; Ma, Q.; Sarkar, A.; Buehler, M. J.; Gracias, D. H. Ultrathin Thermo-responsive Self-Folding 3D Graphene. *Sci. Adv.* **2017**, *3* (10), No. e1701084.
- (14) Miskin, M. Z.; Dorsey, K. J.; Bircan, B.; Han, Y.; Muller, D. A.; McEuen, P. L.; Cohen, I. Graphene-Based Bimorphs for Micron-Sized, Autonomous Origami Machines. *Proc. Natl. Acad. Sci. U. S. A.* **2018**, *115* (3), 466–470.
- (15) Reynolds, M. F.; McGill, K. L.; Wang, M. A.; Gao, H.; Mujid, F.; Kang, K.; Park, J.; Miskin, M. Z.; Cohen, I.; McEuen, P. L. Capillary Origami with Atomically Thin Membranes. *Nano Lett.* **2019**, *19* (9), 6221–6226.
- (16) Davami, K.; Zhao, L.; Lu, E.; Cortes, J.; Lin, C.; Lilley, D. E.; Purohit, P. K.; Bargatin, I. Ultralight Shape-Recovering Plate Mechanical Metamaterials. *Nat. Commun.* **2015**, *6* (1), 1–7.
- (17) Dorsey, K. J.; Pearson, T. G.; Esposito, E.; Russell, S.; Bircan, B.; Han, Y.; Miskin, M. Z.; Muller, D. A.; Cohen, I.; McEuen, P. L. Atomic Layer Deposition for Membranes, Metamaterials, and Mechanisms. *Adv. Mater.* **2019**, *31* (29), 1901944.
- (18) George, S. M. Atomic Layer Deposition: An Overview. *Chem. Rev.* **2010**, *110* (1), 111–131.
- (19) Wang, L.; Travis, J. J.; Cavanagh, A. S.; Liu, X.; Koenig, S. P.; Huang, P. Y.; George, S. M.; Bunch, J. S. Ultrathin Oxide Films by Atomic Layer Deposition on Graphene. *Nano Lett.* **2012**, *12* (7), 3706–3710.
- (20) Eigenfeld, N. T.; Gray, J. M.; Brown, J. J.; Skidmore, G. D.; George, S. M.; Bright, V. M. Ultra-Thin 3D Nano-Devices from Atomic Layer Deposition on Polyimide. *Adv. Mater.* **2014**, *26* (23), 3962–3967.
- (21) Supekar, O. D.; Brown, J. J.; Eigenfeld, N. T.; Gertsch, J. C.; Bright, V. M. Atomic Layer Deposition Ultrathin Film Origami Using Focused Ion Beams. *Nanotechnology* **2016**, *27* (49), 49LT02.
- (22) Benbernou, N.; Demaine, E. D.; Demaine, M. L.; Ovadya, A. A Universal Crease Pattern for Folding Orthogonal Shapes. *0909.5388. ArXiv*, 2009. <https://arxiv.org/abs/0909.5388> (accessed June 7, 2020).
- (23) Demaine, E. D.; Tachi, T. Origamizer: A Practical Algorithm for Folding Any Polyhedron. In *33rd International Symposium on Computational Geometry (SoCG 2017)*; Aronov, B., Katz, M. J., Eds.; Leibniz International Proceedings in Informatics (LIPIcs); Schloss Dagstuhl–Leibniz-Zentrum fuer Informatik: Dagstuhl, Germany, 2017; Vol. 77, pp 34:1–34:16. DOI: 10.4230/LIPIcs.SocG.2017.34.
- (24) Lang, R. J. *Origami Design Secrets: Mathematical Methods for an Ancient Art*, 2nd ed.; CRC Press: Boca Raton, FL, 2011.
- (25) Santangelo, C. D. Extreme Mechanics: Self-Folding Origami. *Annu. Rev. Condens. Matter Phys.* **2017**, *8* (1), 165–183.
- (26) Lang, R. J. *Twists, Tilings, and Tessellations: Mathematical Methods for Geometric Origami*; CRC Press: Boca Raton, FL, 2017.
- (27) Yoshioka, T.; Ando, T.; Shikida, M.; Sato, K. Tensile Testing of SiO₂ and Si₃N₄ Films Carried out on a Silicon Chip. *Sens. Actuators, A* **2000**, *82* (1), 291–296.
- (28) Sharpe, W. N.; Pulskamp, J.; Gianola, D. S.; Eberl, C.; Polcawich, R. G.; Thompson, R. J. Strain Measurements of Silicon Dioxide Microspecimens by Digital Imaging Processing. *Exp. Mech.* **2007**, *47* (5), 649–658.
- (29) Merle, B.; Göken, M. Fracture Toughness of Silicon Nitride Thin Films of Different Thicknesses as Measured by Bulge Tests. *Acta Mater.* **2011**, *59* (4), 1772–1779.
- (30) Al-Halhouli, A. T.; Kampen, I.; Krah, T.; Büttgenbach, S. Nanoindentation Testing of SU-8 Photoresist Mechanical Properties. *Microelectron. Eng.* **2008**, *85* (5), 942–944.
- (31) Lang, R. J. *Robert J. Lang Origami*, 2018. <https://langorigami.com/article/tessellatica> (accessed June 7, 2020).
- (32) Bircan, B.; Miskin, M. Z.; Lang, R. J.; Cao, M. C.; Dorsey, K. J.; Salim, M. G.; Wang, W.; Muller, D. A.; McEuen, P. L.; Cohen, I. *Robert J. Lang Origami* <https://langorigami.com/publication/bidirectional-self-folding-with-atomic-layer-deposition-nanofilms-for-microscale-origami> (accessed June 7, 2020).
- (33) Putkonen, M. Precursors for ALD Processes. In *Atomic Layer Deposition of Nanostructured Materials*; John Wiley & Sons, Ltd, 2012; pp 41–59. DOI: 10.1002/9783527639915.ch3.
- (34) Chen, B. G.; Santangelo, C. D. Branches of Triangulated Origami Near the Unfolded State. *Phys. Rev. X* **2018**, *8* (1), No. 011034.
- (35) Kang, J.-H.; Kim, H.; Santangelo, C. D.; Hayward, R. C. Enabling Robust Self-Folding Origami by Pre-Biasing Vertex Buckling Direction. *Adv. Mater.* **2019**, *31* (39), No. 0193006.
- (36) Cui, J.; Huang, T.-Y.; Luo, Z.; Testa, P.; Gu, H.; Chen, X.-Z.; Nelson, B. J.; Heyderman, L. J. Nanomagnetic Encoding of Shape-Morphing Micromachines. *Nature* **2019**, *575* (7781), 164–168.